VOL. 19, NO. 10, MAY 2024 ISSN 1819-6608

ARPN Journal of Engineering and Applied Sciences

www.arpnjournals.com

DETERMINATION OF CLAY MINERALS IN BRUNEI'S OUTCROPS AND SPATIAL VARIABILITY OF THE RADIOISOTOPES

Amila Abu Bakar, Stephen Tyson and Bashir Busahmin
Department of Petroleum and Chemical Engineering, Faculty of Engineering, University Teknologi Brunei, Jalan Tungku Link, BE, Gadong, Brunei Darussalam
E-Mail: Milafashihah@gmail.com

ABSTRACT

Shale with the presence of clay minerals is one of the problematic formations to be encountered in the oil and gas industry. Drilling into these formations will be a challenge since shale sloughs and clay swells. Clay minerals impact hydrocarbon production and drilling operations due to clay hydration. Thus, the main objective of this paper is to identify the clay minerals from Brunei Darussalam outcrops based on the cross plot of thorium and potassium from the components of the radioisotopes of spectral gamma ray logging (SGRL). The majority of the outcrops in Brunei Darussalam contains montmorillonite which swell in contact with water. Geostatistical methods are implemented to gather spatial data over an area of interest. Variogram therefore is used to describe and characterize the variability of the radioisotopes by fitting a model to the experimental semi-variogram. The estimation of the measured values at any unknown location are then calculated by the kriging process. Semi variogram and corresponding kriging maps for thorium, uranium, and potassium components were prepared. The result indicated a good spatial similarity and areas with the highest number of the radioisotopes of spectral gamma ray logging presented the relationship of the radioisotopes in the surrounding area.

Keywords: clay, spatial variability, swelling, variogram, kriging.

Manuscript Received 30 March 2024; Revised 18 June 2024; Published 10 August 2024

1. INTRODUCTION

In the oil and gas industry, shale is one of the problematic formations to be encountered, more than 75% of world drilling operations problems are related to shale formation. Despite various studies being made on shale stability, it is still a challenge to fully understand the mechanisms involved in shale [1, 2, 3]. Shales contain clay minerals such as montmorillonite that swell which can impact hydrocarbon production and drilling operations. Such problems can be foreseen on account of clay element composition identification based on the components of radioisotopes of the spectral gamma ray log (SGRL). It is widely used for lithology determination, geological assessment of determination of clay and the evaluation of clay mineralogy [4]. In addition, the assessment of the spatial variation of the radioisotopes is carried out to predict the values at unsampled locations. Brunei Darussalam is in the in the northern part of the Borneo Island and has unconsolidated sandstone reservoirs in shallow marine environment. Figure-1 shows the lithostratigraphy of Brunei where the geological age of Brunei is relatively young from Pliocene to Late Miocene in the Cenozoic basin, where it is composed of three major delta systems: Baram, Champion, and Meligan Deltas.

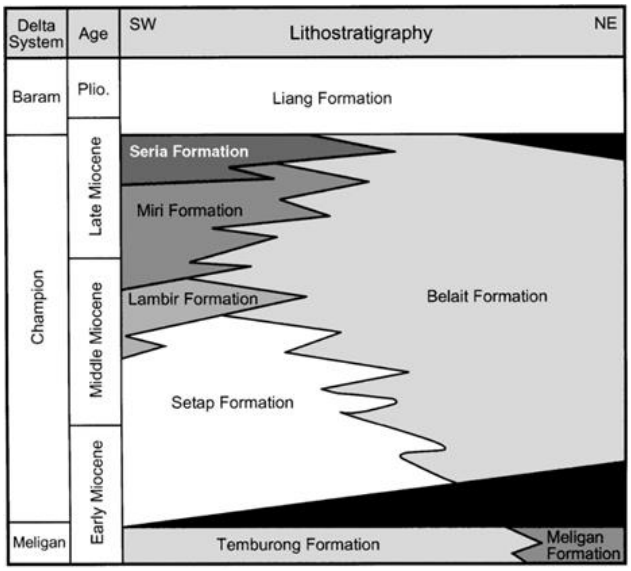

Figure-1. Lithostratigraphy of Brunei, adapted from [5].

Clay minerals in Brunei Darussalam were characterised into outcrops and offshore clay minerals with different properties that influence the properties of the formation. Limited studies have been made on the characterization of clay in Brunei Darussalam; however [6] studied the description of clay minerals from samples collected in Belait and Liang formation in Lumut and Berakas member. It was found that only illlite and chlorite are present in Belait formation. For Liang formation, Lumut member, clay minerals such as kaolinite, illite and chlorite was found. Within the Berakas member, only kaolinite and illite was found which matches the outcome for Liang

ARPN Journal of Engineering and Applied Sciences

www.arpnjournals.com

formation in outcrops of Central Sarawak, Malaysia [7]. In terms of offshore clay minerals, it is based on the lithology from Labuan in Malaysia as it is a representative of offshore Belait formation in Brunei Darussalam [8]. It has been observed that the outcrops contained clay that was mostly chlorite, kaolinite with some mixed-layer and montmorillonite [9, 10]. Furthermore, geostatistics such as variogram and kriging modelling are implemented to study the spatial variability of the clay. The variogram is to describe the relationship of thorium, potassium, and uranium while kriging modelling is to predict the presence of clay based on interpolation methods. Thus, the objective of this paper is to identify the primary clay minerals using spectral gamma ray log.

2. METHODOLOGY

A total of six outcrop locations were visited and samples were collected for the analysis. RS-332 hand-held multipurpose gamma-ray spectrometer system from Radiation Solution inc. is utilized to measure the total gamma-ray in API and spectral gamma ray readings. The Assay mode is used for measurement of the radioisotopes; concentration of thorium (ppm), potassium (%) and uranium (pm). The data obtained is then plotted in a cross-plot of thorium to potassium ratio to determine the clay minerals as presented in Figure-2 and Table-1.

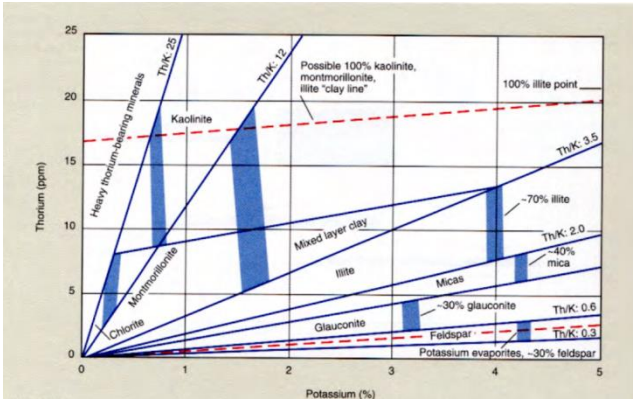

Figure-2. The cross plot of thorium to potassium ratio [11].

Table-1. The thorium to potassium ratio [11].

Th/K (ppm/%)	Clay minerals
< 0.3	Potassium evaporites
0.3 – 0.6	Feldspars
0.6 – 1.5	Glauconite
1.5 – 2.0	Micas
2.0 – 3.5	Illite
> 3.5	Mixed-layer clays
10 and above	Kaolinite and Chlorite

In terms of spatial variability of clay, the first step is to build the semi-variogram model to determine the relationship of variability with the distance and followed by constructing kriging model to interpolate the radioisotopes components such as potassium, thorium, and uranium over an area of interest. Variogram analysis is used to describe and characterize the variability of measurement.

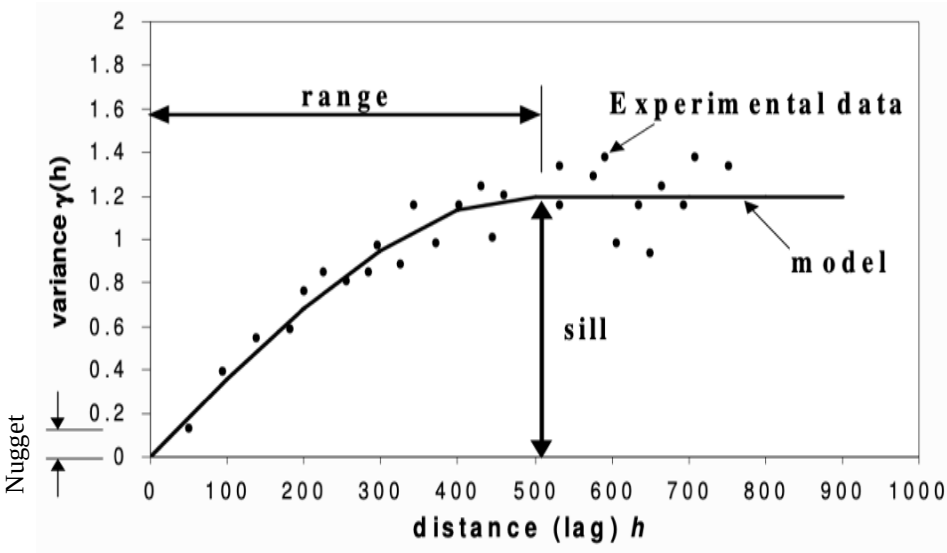

Figure-3. Variogram plot [12].

In addition, the variogram analysis consists of the data from the experimental variogram and the variogram model fitted to the data. Figure-3 presents the plot of variability for several distance intervals that represents the autocorrelation. The variogram model is chosen from a set of mathematical functions that describe the spatial relationship as tabulated in Table-2. Moreover, the range of point-to-point distances within the data points are related to one another, whereas the distance increases, the variability increased. At some points, the distance between the data points is great enough; the points are no longer related to one another. This can be seen as a horizontal line which is known as sill; therefore, nugget is a semi variance when the lag distance is zero. Furthermore, the root mean squared error (RMSE) is calculated for each variogram model to measure the difference between the actual and the predicted values. Equation 2.1 shows how the RMSE is calculated.

Table-2. Details of different variogram models [13,14].

Variogram models	Equation
Spherical	$\gamma(\|h\|) = C_o + C\left[1.5\left(\frac{\|h\|}{a}\right) - 0.5\left(\frac{\|h\|}{a}\right)^3\right]$, for $0 < \|h\| < a$ $\gamma(\|h\|) = C_o + C$, for $\|h\| > a$ $\gamma(\|h\|) = C_o$, for $\|h\| = 0$ where, a is the range. C_o is the nugget effect C is the sill value
Exponential	$\gamma(\|h\|) = C_o + C\left(1 - e^{\frac{-3\|h\|}{a}}\right)$
Gaussian	$\gamma(\|h\|) = C_o + C\left(1 - e^{-\frac{3h^2}{a^2}}\right)$
Cubic	$\gamma(\|h\|) = C_o + C\left(7\left(\frac{h^2}{a^2}\right) - \frac{35}{4}\left(\frac{h^3}{a^3}\right) + \frac{7}{2}\left(\frac{h^5}{a^5}\right) - \frac{3}{4}\left(\frac{h^7}{a^7}\right)\right)$
Stable	$\gamma(\|h\|) = C_o + C\left(1 - e^{-\frac{h^s}{a}}\right)$ where, s is the shape parameter

$$RMSE = \sqrt{\frac{1}{n}\sum_{i=1}^{n}(P_i A_i)^2} \quad (2.1)$$

whereas,
P_i is the predicted value.
A_i is the actual value.
n is the total sample size

Once the semi-variogram is known, the estimation of the measured values at any unknown location is performed by kriging process. The estimated value for ordinary kriging at a given location is the sum of the values at known locations multiplied by weight as shown in equation 2.2. The weights can be calculated using matrix equation. All the steps are executed using Python software.

$$z^*_{OK}(\mu) = \sum_{i=1}^{n(\mu)} \lambda_i^{OK}(\mu) \cdot z(\mu_i) \quad (2.2)$$

3. RESULT AND DISCUSSIONS

Cross plot of Thorium to Potassium are plotted to identify the clay minerals. Histograms are also shown to visualize the dominating clay minerals. Table-3 shows the results for all six outcrops. All six outcrops have varying thorium to potassium ratio as illustrated in Figure-4 and Figure-5. All outcrops have montmorillonite and only some location shows the presence of kaolinite. For Dare and JL, only Montmorillonite is present which can swell when is in contact with water, hence the hydrocarbon production is negatively affected as well as the operating drilling parameters are reduced due to the change in the clay content and the results aligned with [15,16].

ARPN Journal of Engineering and Applied Sciences

Table-3. Outcrops data for clay mineral identification.

No.	Outcrops			
	Location	**Th/K ranges**	**Types of clay minerals**	**Lithology**
1	Dare Industrial Park, Terunjing (Dare)	5.605 - 11.130	Montmorillonite	Belait Formation
2	Landfill Station, Sungai Akar (SA)	5.785 - 20.336	Montmorillonite and Kaolinite	
3	Lumapas Outcrop near Bukit Saeh (LQ)	6.217 - 16.402	Montmorillonite and Kaolinite	
4	Bukit Silat, Kampong Katok B (BS)	5.702 - 14.097	Montmorillonite and Kaolinite	Miri Formation
5	Tanjong Nangka (TN)	4.966 - 12.165	Montmorillonite and Kaolinite	
6	Simpang 581, Jalan Lamunin (JL)	5.922 - 10.692	Montmorillonite	

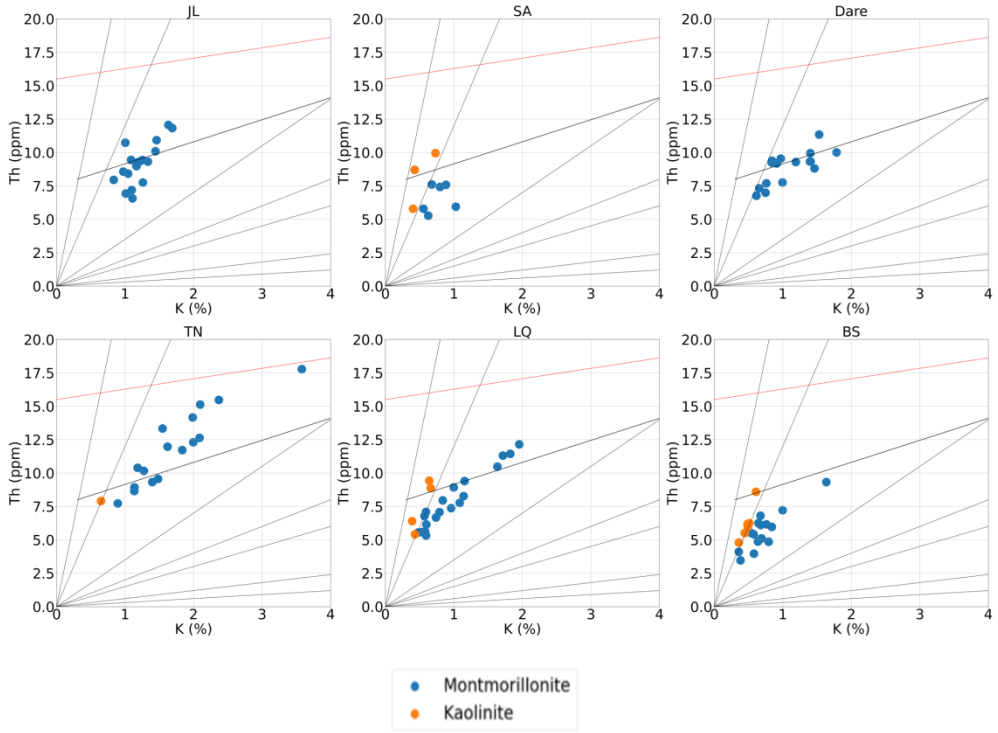

Figure-4. The cross plot of thorium to potassium ratio for outcrops data.

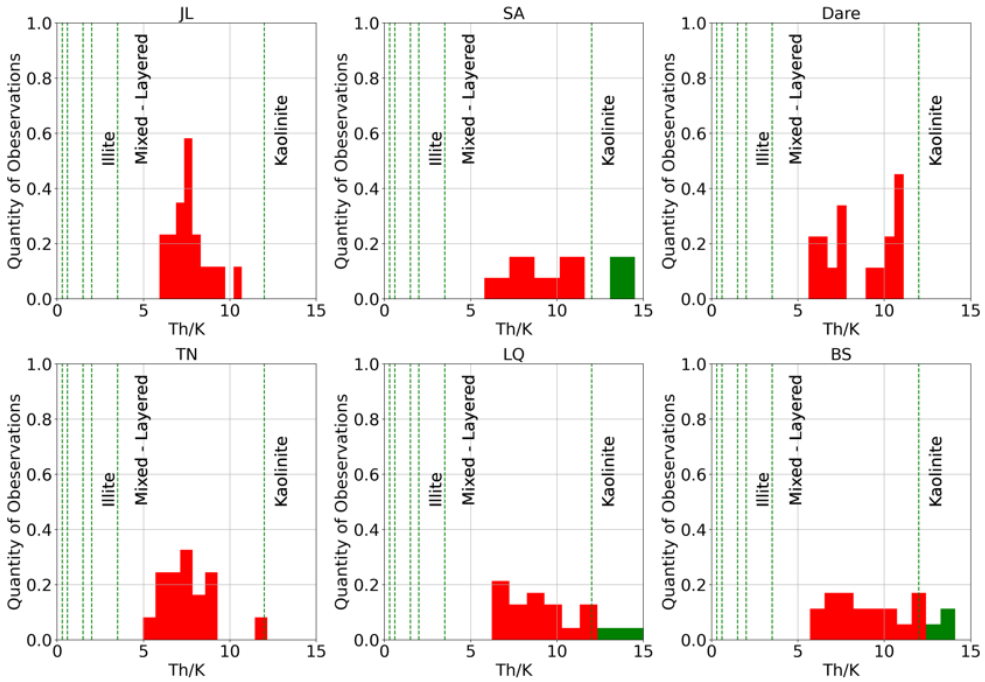

Figure-5. The histogram plot for six outcrops.

For spatial variability of clay, a variogram model is first chosen from sets of mathematical functions. The process in fitting a model to the experimental semi variogram is based on a trial-and-error method. The most appropriate model is chosen by matching the shape of the curve from the experimental semi variogram to the mathematical function. Table-4 displayed the outcome from selecting the most suitable variogram model for each radioactive component (potassium, thorium, and uranium). Based on the analysis, for potassium concentration, all the 5 models described the experimental variogram equally well in terms of RMSE. However, the spherical model has the highest effective range of 199.98 and as seen in Figure-6, the model is forming almost a horizontal line. The rest of the four models (exponential, gaussian, cubic and stable) all seem to have a similar semi variogram plot. As for uranium and thorium concentration, a similar outcome can be seen from potassium concentration where the RMSE is all equal to 0.090 and 0.91 respectively.

Table-4. Various variogram models for potassium, uranium, and thorium.

	Variogram models	Effective Range	Sill	Nugget	Root mean square error
For potassium concentration	Spherical	199.98	0.028	0.059	0.035
	Exponential	43.45	0.082	0	0.033
	Gaussian	41.09	0.064	0.018	0.033
	Cubic	49.67	0.064	0.017	0.033
	Stable	35.58	0.064	0.017	0.033
For uranium concentration	Variogram models	Effective Range	Sill	Nugget	Root mean square error
	Spherical	76.06	0.045	0.21	0.090
	Exponential	66.65	0.049	0.20	0.091
	Gaussian	71.77	0.040	0.21	0.090
	Cubic	90.00	0.040	0.21	0.090
	Stable	62.14	0.040	0.21	0.090
For thorium concentration	Variogram models	Effective Range	Sill	Nugget	Root mean square error
	Spherical	39.03	1.80	0.78	0.91
	Exponential	36.88	2.28	0.31	0.91
	Gaussian	36.71	1.57	1.01	0.91
	Cubic	45.28	1.55	1.02	0.91
	Stable	35.07	1.93	0.65	0.91

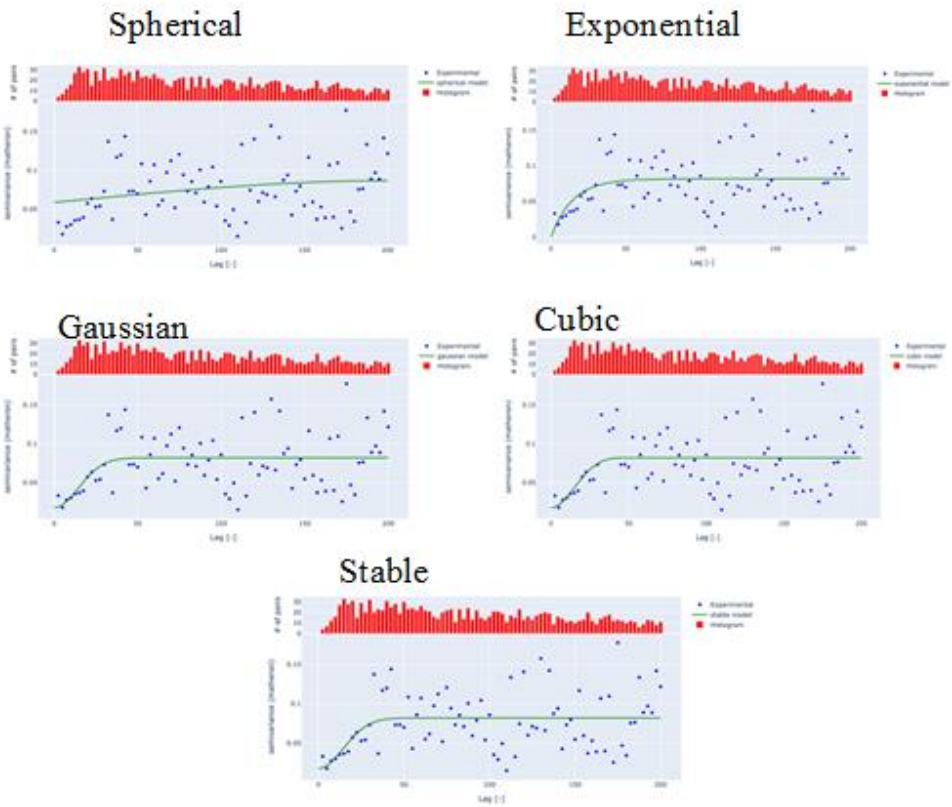

Figure-6. The comparison of the theoretical models for potassium concentration.

Once the semi variogram is known, the estimation of the measured values at any unknown location can be done by kriging process. Based on the interpolation for potassium component, 3422 locations are found, and extrapolation were made with the ordinary kriging model. As seen on Figure-7, the error estimation plot, the error increases in areas with lower density of measurement. A comparable result can be seen for thorium concentration where 7972 locations are found. As for uranium concentration, a slightly different interpolation pattern. Only 367 locations are found, and the interpolation cover a wide range of area as shown in Figure-8. It can be concluded that the outcome from this analysis is highly dependent on the sampling data.

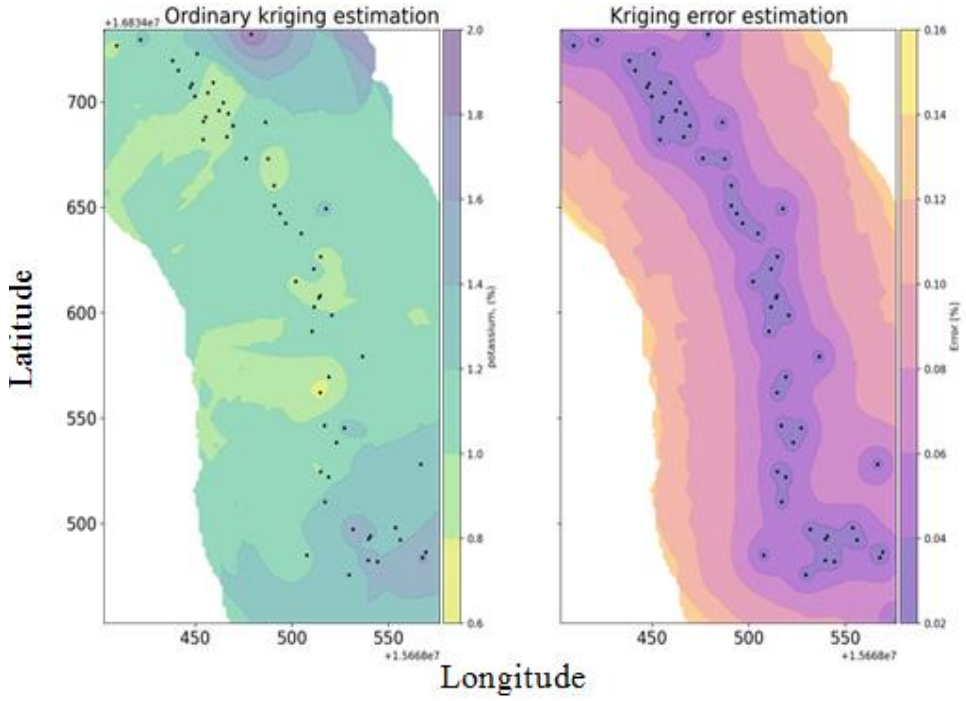

Figure-7. The ordinary kriging with its error estimation for potassium concentration.

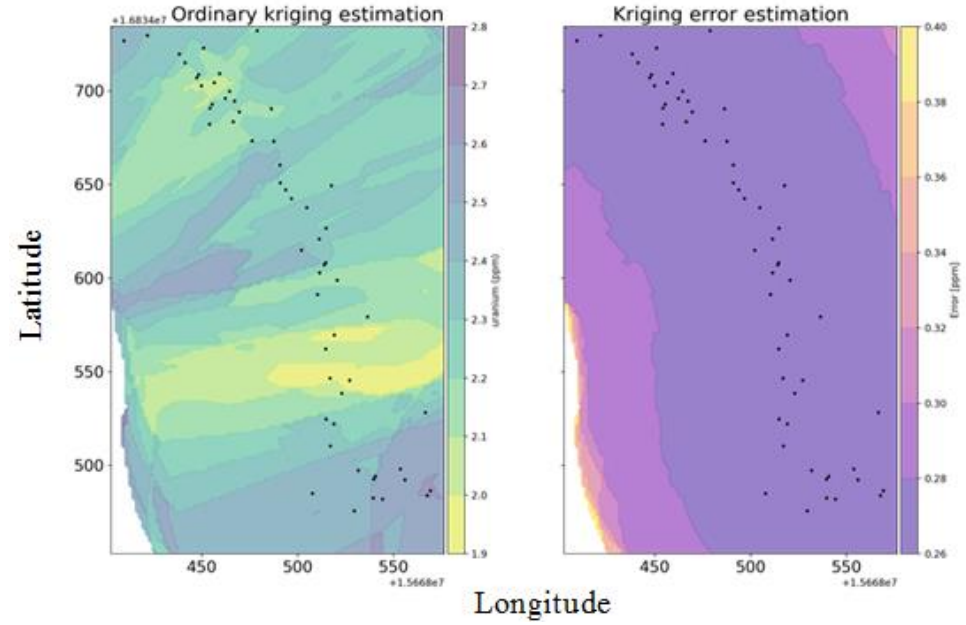

Figure-8. The ordinary kriging with its error estimation for uranium concentration.

4. CONCLUSIONS

Spectral gamma ray log (SGRL) presents an attractive potential in identifying clay minerals. From the analysis, for each outcrops area, their cross plot and histogram are plotted. Most clay minerals detected include montmorillonite, mixed layer clays and kaolinite. To further

utilize the spectral gamma ray log, geostatistical method was implemented to gather a spatial data over an area of interest which provides a framework of values at yet-to-be tested location based on the spatial correlation of the radioisotope's components. A good and similar spatial distribution can be seen from the radioisotope's component as greater error in the areas with lower density of measurement.

Overall, this paper provides the capability of SGRL in determining the clay minerals based on the cross plot of thorium and potassium as well as its application.

REFERENCES

[1] Chukwuemeka A.O., Amede G. and Alfazazi U. 2017. A review of wellbore instability during well construction: Types, causes, prevention, and control. Petroleum and Coal. 59(5): 590-610.

[2] Wilson M.J. and Wilson L. 2014. Clay mineralogy and shale instability: an alternative conceptual analysis. Clay Minerals, 49(2): 127-145. doi: https://doi.org/10.1180/claymin.2014.049.2.01.

[3] Okafor I.S., Joel O.F., Iyuke S.E., Ubani C.E. and Ndubuisi E.C. 2017. Effect of Shale Properties on Wellbore Instability during Drilling Operations: A Case Study of Selected Fields in Niger Delta-Nigeria. International Journal of Petroleum and Petrochemical Engineering (IJPPE), 3(1): 22-30. doi: http://dx.doi.org/10.20431/2454-7980.0301003.

[4] Rahmat Catur Wibowo, Alia Puja Pertiwi and Suci Kurniati. 2020. Identification of Clay Mineral Content Using Spectral Gamma Ray on Y1 Well in Karawang Area, West Java, Indonesia. Journal of geoscience, engineering, environment, and technology, 5(3): 153-160. doi: https://doi.org/10.25299/jgeet.2020.5.3.4504.

[5] Curiale J., Morelos, J., Lambiase, J. and Mueller, W. 2000. Brunei Darussalam: Characteristics of selected petroleums and source rocks. Organic Geochemistry, 31(12): 1475-1493. doi: https://doi.org/10.1016/S0146-6380(00)00084-X.

[6] Karim K.N., N.F.N. and Ifandi E. 2017. Characterization of clay minerals in Liang, Belait and Seria Formations and modern offshore sediments, Brunei Darussalam. The 1st International congress on earth sciences.

[7] Amirah Khairiyah Johari, Bashir Busahmin, Stephen Tyson, Prediction of Spatial Variability in Grain Size Distribution on Outcrop from Gamma Ray, Petroleum & Coal, 66(3): 914-922.

[8] Ibrahim W.E., Salim A.M.A. and Sum C.W. 2019. Mineralogical investigation of fine clastic rocks from Central Sarawak, Malaysia. Journal of Petroleum Exploration and Production Technology, 10(1): 21-30. doi: https://doi.org/10.1007/s13202-019-00751-0.

[9] Lukie T. and Balaguru A. 2012. Sequence Stratigraphic, Sedimentologic and Petrographic Insights of the Miocene (Stage IVA) Outcrops of the Klias Peninsula and Labuan Island, Sabah, Malaysia, Borneo. AAPG Bulletin.

[10] Kessler F.L. and Jong J. 2015. Tertiary Uplift and the Miocene Evolution of the NW Borneo Shelf Margin. Berita Sedimentologi- Indonesian Journal of Sedimentary Geology. 33: 21-46.

[11] Risha M. and Douraghi J. 2021. Impact of Clay mineral type on sandstone permeability based on field investigations: case study on Labuan Island, Malaysia. Journal of Physics: Conference Series. doi: http://dx.doi.org/10.1088/1742-6596/1818/1/012091.

[12] Klaja J. and Dudek L. 2016. Geological interpretation of spectral gamma ray (SGR) logging in selected boreholes. Nafta-Gaz, 72(1): 3-14. doi: https://doi.org/10.18668/ng2016.01.01.

[13] Kapur B., Pasquale S., Tekin S., Todorovic M., Sezen S., Özfidaner M. and Gümüş Z. 2010. Prediction of climatic change for the next 100 years in Southern Italy. Scientific Research and Essays. 5(12): 1470-1478.

[14] Rashad M.Z., El-Qady G. and Ushijima K. 2000. Selection of variogram models. 60(3): 105-116.

[15] Ahram Kim, Bashir Busahmin and Stephen Tyson Compositional Kriging Analysis: A Spatial Interpolation Method for Distribution, Publication date, 2024/1, 19(1): 1819-6608, 9-14, Asian Research Publishing Network (ARPN).

[16] Ahram Kim, Bashir Busahmin and Stephen Tyson Prediction of Grain Size Distribution using Ordinary Kriging and Composition Kriging Methods. Publication date, 2024, 19(9), pp. 556–562. Asian Research Publishing Network (ARPN).